
COLONFORMER: AN EFFICIENT TRANSFORMER BASED METHOD FOR COLON POLYP SEGMENTATION

A PREPRINT

Nguyen Thanh Duc

School of Information and Communication Technology
Hanoi University of Science and Technology
duc.nt170058@sis.hust.edu.vn

Nguyen Thi Oanh

School of Information and Communication Technology
Hanoi University of Science and Technology
oanhnt@soict.hust.edu.vn

Nguyen Thi Thuy

Faculty of Information Technology
Vietnam National University of Agriculture
ntthuy@vnua.edu.vn

Tran Minh Triet

University of Science
Vietnam National University Ho Chi Minh City
tmtriet@fit.hcmus.edu.vn

Dinh Viet Sang *

School of Information and Communication Technology
Hanoi University of Science and Technology
sangdv@soict.hust.edu.vn

June 8, 2022

ABSTRACT

Identifying polyps is challenging for automatic analysis of endoscopic images in computer-aided clinical support systems. Models based on convolutional networks (CNN), transformers, and their combinations have been proposed to segment polyps with promising results. However, those approaches have limitations either in modeling the local appearance of the polyps only or lack of multi-level feature representation for spatial dependency in the decoding process. This paper proposes a novel network, namely ColonFormer, to address these limitations. ColonFormer is an encoder-decoder architecture capable of modeling long-range semantic information at both encoder and decoder branches. The encoder is a lightweight architecture based on transformers for modeling global semantic relations at multi scales. The decoder is a hierarchical network structure designed for learning multi-level features to enrich feature representation. Besides, a refinement module is added with a new skip connection technique to refine the boundary of polyp objects in the global map for accurate segmentation. Extensive experiments have been conducted on five popular benchmark datasets for polyp segmentation, including Kvasir, CVC-Clinic DB, CVC-ColonDB, CVC-T, and ETIS-Larib. Experimental results show that our ColonFormer outperforms other state-of-the-art methods on all benchmark datasets.

Keywords Semantic segmentation · Deep learning · Encoder-decoder network · Polyp segmentation · Colonoscopy

1 Introduction

Colorectal cancer (CRC) is among the most common types of cancer worldwide, causing over 694,000 fatalities each year [1]. The most common cause of CRC is colon polyps, particularly adenomas with high-grade dysplasia. According to a longitudinal study [2], every 1% increase in adenoma detection rate is linked to a 3% reduction in the risk of colon cancer. As a result, detecting and removing polyps at an early stage is critical for cancer prevention and

*Corresponding author

treatment. Therefore, colonoscopy is regarded as the standard tool for detecting colon adenomas and colorectal cancer. In practice, overburdened healthcare systems, particularly in low-resource settings, may result in shorter endoscopy durations and more missed polyps. According to a literature review, the proportion of colon polyps missing during endoscopies could range from 20 to 47 percent [3]. This may lead to high associated risk factors in patients. Therefore, research in developing computer-aided tools to assist endoscopists in endoscopy procedures is an essential need.

Advancements in artificial intelligence and deep learning have changed the landscape of such systems. Attempts have been made to develop learning algorithms to deploy in computer-aided diagnostic (CAD) systems for the automatic detection and prediction of polyps, which could benefit clinicians in detecting lesions and lower the miss detection rate [4, 5, 6]. Deep neural networks have shown great potential in assisting colon polyp detection in several retrospective investigations and diagnoses. A CAD system can support endoscopists in improving lesion detection rates, optimizing strategies during endoscopy for high-risk lesions, and increasing clinics' capacity while preserving diagnostic quality [7, 8].

Despite progress in machine learning and computer vision research, automatic polyp segmentation remains a challenging problem. Polyps are caused by abnormal cell growth in the human colon, meaning their appearances have strong relationships with the surroundings. Images of polyps come in various shapes, sizes, textures, and colors. In addition, the boundary between polyps and their surrounding mucosa is not always apparent during colonoscopy, especially in different lighting modes and in cases of flat lesions or unclear bowel preparation. These cause a lot of uncertainty for the learning models for polyp segmentation.

In recent years, the most widely used methods for image segmentation in general and polyp segmentation, in particular, are based on Convolutional Neural Networks (CNNs). Most segmentation models use a UNet-based architecture containing an encoder and a decoder, which are often built up from convolutional layers. Despite being widely used for segmentation tasks with impressive performance, CNNs pose certain limitations: They can only capture local information while ignoring spatial context and global information due to the limited receptive field. Furthermore, it was shown that CNNs act like a series of high-pass filters and favor high-frequency information.

Transformer [9] is a recently proposed deep neural network architecture that models the global interactions among input components using attention mechanisms. While initially designed to tackle natural language and speech processing problems, Transformers have significantly impacted computer vision in recent years. In contrast to CNNs, self-attention layers in Transformers work as low-pass filters, and they can effectively capture long-range dependency. Therefore, combining the strengths of convolutional and self-attention layers can increase the representation power of deep networks. Very recently, there has been fast-growing interest in using Transformers for semantic image segmentation [10, 11, 12, 13]. These methods use well-known encoder-decoder architectures wherein Transformers and CNNs are combined in various settings. The works in [10, 11, 12] proposed Transformer-CNN architectures, in which a Transformer is used as an encoder, and a traditional CNN is used as a decoder. The hybrid architecture of Transformers and CNN has been proposed in [13], in which the decoder is a traditional CNN or a Transformer, while the encoder is a combination of CNN and Transformer layers.

Inspired by these approaches for modeling multi-scale and multi-level features, we propose a new Transformers-based network called ColonFormer. The main design of our ColonFormer also contains a transformer encoder and a CNN decoder, but our approach is different from the models mentioned above in several ways. In ColonFormer, the encoder is a hierarchically structured lightweight Transformer for learning multi-scale features. The decoder is a hierarchical pyramid structure with the capability of learning from heterogeneous data containing feature maps extracted from encoder blocks at different scales and subregions. Besides, a refinement module is proposed for further improving the segmentation accuracy on hard regions and small polyps.

Our main contributions include:

- A novel deep neural network, namely ColonFormer, that integrates a hierarchical Transformer and a hierarchical pyramid CNN in a unified architecture for efficient and accurate polyp segmentation;
- An improved refinement technique using a newly proposed residual axial attention module for feature fusion and smoothing aiming at improving the segmentation accuracy;
- A set of experiments on five standard benchmark datasets for polyp segmentation (Kvasir, CVC-Clinic DB, CVC-ColonDB, CVC-T, and ETIS-Larib) and comparisons of the effectiveness of ColonFormer to current state-of-the-art methods.

The rest of the paper is organized as follows. We provide a brief review of related works in Section 2. The ColonFormer architecture is described in Section 3. Section 4 presents our experiments and results. Finally, we conclude the paper and highlight future works in Section 5.

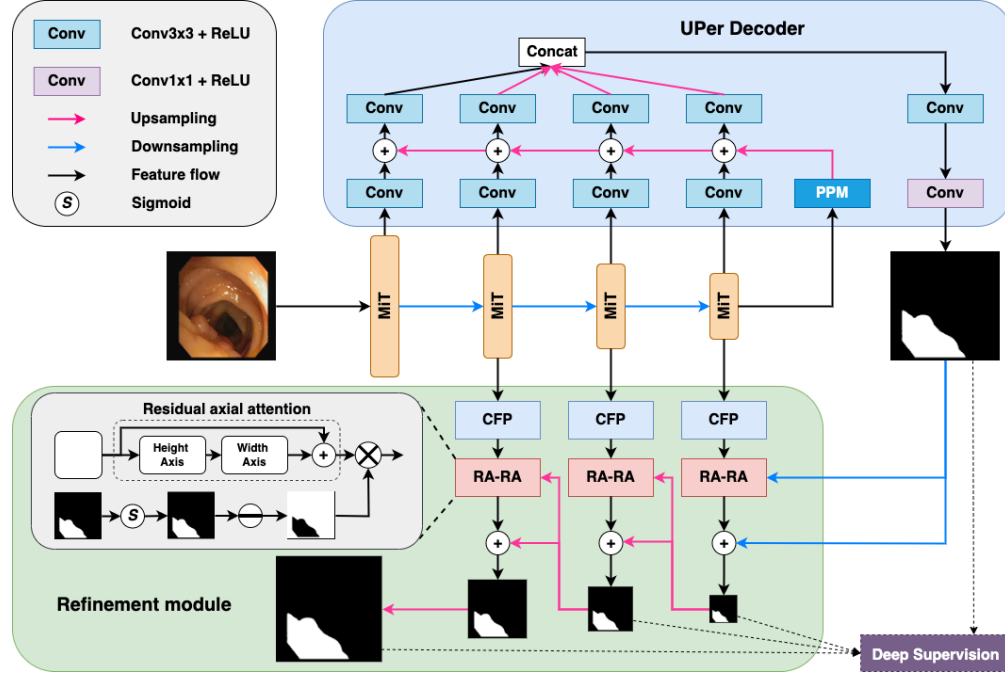


Figure 1: The overall architecture of our ColonFormer contains three components: an encoder, a decoder, and a refinement module. The encoder is based on the Mix Transformer backbone. The decoder starts with a pyramid pooling module (PPM), where its outputs are combined layer-wise with the output feature maps of the encoder at multi levels to produce a global map. The refinement module aims to gradually refine the boundary of the global map to yield the final accurate segmentation. Besides this predicted output, the global map and two intermediate maps are also passed into the training loss in a deep supervision manner. Before calculating the training loss, all refined maps are upsampled back to the original image input size.

2 Related Work

In this section, we briefly review common methods and techniques that have been developed for polyp segmentation. We review CNN architectures and their variants, especially UNet models, in medical image segmentation. Then we investigate the attention mechanism as a promising technique that boosts the capability of a deep neural network in learning feature representation. Finally, vision Transformer and its applications in polyp segmentation and medical image processing are investigated.

2.1 Convolutional Neural Networks

CNNs are one of the most widely used deep neural network architectures, especially in computer vision. A deep CNN extracts features on multiple layers with increasing levels of abstraction. Low-level features with high resolutions represent spatial details, while high-level features with low resolutions represent rich semantic information. CNNs are especially powerful in image analysis as they can extract highly informative and valuable features.

UNet [14] is a pioneering CNN architecture for medical image segmentation. UNet consists of an encoder and a decoder. The encoder includes convolutional, pooling layers for feature extraction, and the decoder uses upsampling (or deconvolutional) and convolutional layers for yielding the final segmentation prediction. Later works attempted to improve UNet by introducing skip connections, which alleviate information loss caused by stacking multiple convolutional layers. However, retaining information from low-level may introduce noisy signals that degrade the performance. UNet variants such as UNet++ [15] and DoubleUNet [16] have achieved stellar results on segmentation benchmarks. UNet++ is constructed as an ensemble of nested UNets of varying depths, which partially share an encoder and jointly learn using deep supervision. DoubleUNet stacks two UNet blocks and uses ASPP [17], and SE blocks [18] to enhance the feature representation.

UNet encoders often use an existing pretrained architecture, also known as the backbone. Widely used backbones include VGG [19], MobileNet [20], ResNet [21], DenseNet [22], etc. PraNet [23] uses Res2Net as the backbone,

while AG-CuResNeSt [24] uses ResNeSt. Meanwhile HarDNet-MSEG [25], NeoUNet [26] and BlazeNeo [27] use HarDNet, an improvement of DenseNet to extract features.

2.2 Attention Mechanism

The attention mechanism is a widely used technique to help deep neural networks learn better feature representations, especially on highly variant inputs. Oktay et al. [28] proposed an Attention Gate module for UNet, which helps the model focus on necessary information while preserving computational efficiency. AG-ResUNet++ [29] integrates the attention gates with the ResNet backbone to improve UNet++ [15] for polyp segmentation. PraNet [23] uses the Reverse Attention module [30], which enforces focus on the boundary between a polyp and its surroundings. In general, most CNNs and neural networks can benefit by adding attention modules. However, even with these attention mechanisms, CNNs are limited by the locality of convolution operations. This limitation makes them difficult to model natural long-range spatial dependencies between input segments.

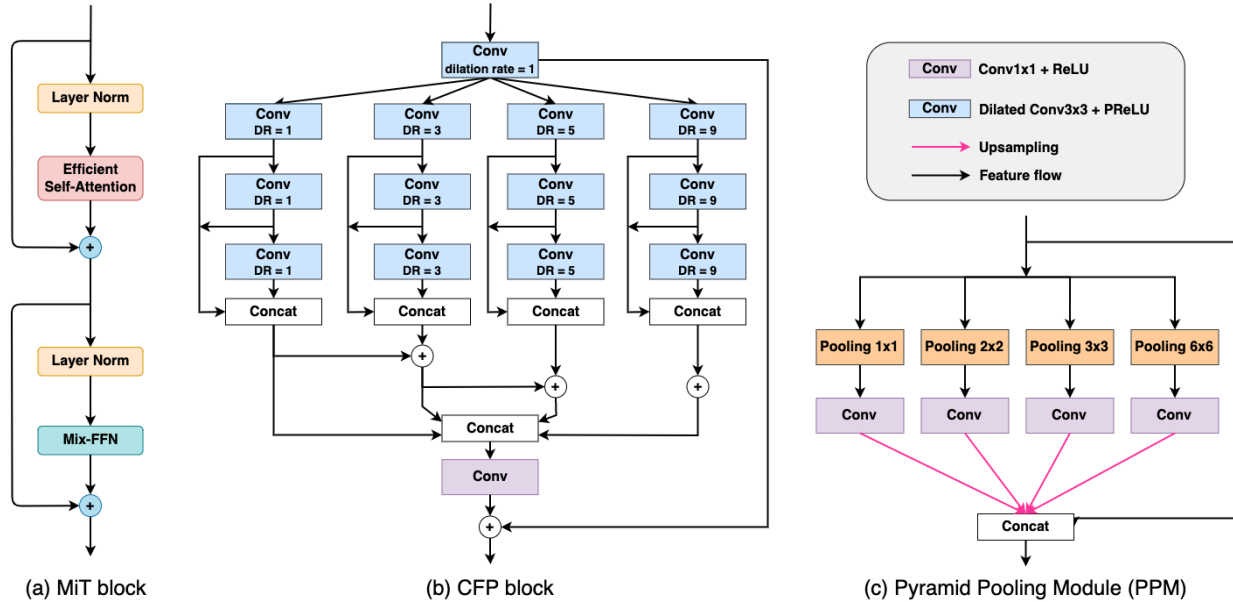


Figure 2: The architecture of three neural blocks used in our ColonFormer. The left block (a) is the Mix Transformer block [31]. The middle block (b) is the channel-wise feature pyramid block. The pyramid pooling module is shown on the right (c). Here DR stands for dilation rate.

2.3 Vision Transformer

Transformer [9] is a highly influential deep neural network architecture, originally proposed to solve natural language processing and similar problems. While the original Transformer architecture is not very well suited for image analysis, attempts have been proposed to leverage its advantages for computer vision through some modifications. Vision Transformer (ViT) [32] was the first successful application of Transformers for computer vision. ViT splits an image into patches and processes them as sequential tokens. This method greatly reduces computational costs and allows Transformers to work with large images feasibly.

A major issue of ViT is that it requires extensive datasets for training to remain effective while being severely limited when trained on small datasets. Such property hinders its usage in problems such as medical image analysis, including polyp segmentation, where data is typically scarce. The Kvasir dataset, for example, contains just 1000 images and their corresponding ground truth, despite being the largest public image dataset of the gastrointestinal tract for polyp segmentation.

Recent works have attempted to further enhance ViT in several ways. DeiT [33] introduces a data-efficient training strategy combined with a distillation approach, which helps improve the performance when training on small datasets. Swin Transformer [10] redesigned the encoder for Transformers. The Swin Transformer encoder computes self-attention among a collection of adjacent patches within a sliding window. Patches are merged every few blocks, reducing the number of tokens and forming a multi-resolution token hierarchy similar to convolutional blocks. Seg-

Former [31] is another hierarchical Transformer design, where patches are merged with overlap and preserving local continuity around patches. The authors also introduced Efficient Self-Attention, a modified attention mechanism for reducing computational complexity, and Mix-FFN for better positional information.

Both TransUNet [34] and TransFuse [35] models have been developed based on Transformers for polyp segmentation and yielded promising results. TransUNet uses a Transformer-based network with a hybrid ViT encoder and upsampling CNN decoder. The Hybrid ViT stacks the CNN and Transformer together, leading to high computational costs. TransFuse addressed this problem by using a parallel architecture. Both models use the attention gate mechanism [28] and a so-called BiFusion Module. These components make the network architecture large and highly complex.

While there have been promising results in using Transformers to develop networks for polyp segmentation, there is plenty of room for improvement in this direction. Most notably, reduced network size and latency can greatly benefit downstream applications. In addition, improved accuracy and robustness can also be achieved with more optimized architectures. This paper seeks to design a Transformer-based architecture that achieves these goals.

3 ColonFormer

Fig. 1 depicts the overall architecture of our proposed network, ColonFormer. The network consists of a hybrid encoder, a decoder, and a refinement module. We will describe each component in detail in the following sections.

3.1 Encoder

A hierarchically structured model that can extract coarse-to-fine features at multi-scale and multi-level is desired for semantic segmentation. Our model uses Mix Transformer (MiT) proposed in [31] as the encoder backbone. MiT is a hierarchical Transformer encoder that can represent both high-resolution coarse and low-resolution fine features. Assume $X \in \mathbb{R}^{H \times W \times C}$ denotes the input image. MiT generates the CNN-like multi-level features F_i . The hierarchical feature map F_i has the resolution of $\frac{H}{2^{i+1}} \times \frac{W}{2^{i+1}} \times C_i$, where $i \in \{1, 2, 3, 4\}$ and C_i is ascending. The hierarchical feature representation is brought by the overlapped patch merging. After several Transformer blocks (Fig. 2a), a kernel with a stride smaller than kernel size is used to divide the feature map into overlapping patches. Such an overlapping patch merging process ensures the local continuity around those patches.

Like other Transformer blocks, MiT blocks contain three main parts: Multi-head Self-Attention (MHSA) layers, Feed Forward Network (FFN), and Layer Norm. The MHSA is improved into Efficient Self-Attention, where the number of keys is decreased by a factor of R to reduce the computational complexity of self-attention layers. Another reason that we decide to choose MiT is the Mix-FFN. Instead of using the positional encoding (PE) as ViT, a 3×3 convolution kernel is integrated into FFN. Since the resolution of PE is fixed, it can not utilize the positional information of the pretrained dataset like ImageNet when test resolution differs from the training one. In such cases, ViT [32] suggests interpolating the PE, which can lead to a drop in accuracy. In contrast, arguing that convolutional layers are adequate for providing location information for Transformer, MiT directly uses a 3×3 convolutional layer for positional encoding. MiT has a series of variants, from MiT-B1 to MiT-B5, with the same architecture but different sizes. We name the variants of our model as **ColonFormer-XS**, **ColonFormer-S**, **ColonFormer-L**, **ColonFormer-XL**, **ColonFormer-XXL**, corresponding to different MiT backbone scales from MiT-B1 to MiT-B5, respectively. According to ablation study described later in Section 4.4, we found that ColonFormer-S and ColonFormer-L achieve the best results. Therefore, we mostly use ColonFormer-S and ColonFormer-L for comparison with other state-of-the-arts in all experiments except where it is specified otherwise.

3.2 Decoder

In order to further capture global context information, the feature maps extracted from the final block of the encoder are first processed by a Pyramid Pooling Module (PPM) [36] before being passed through the decoder blocks. The PPM simultaneously produces multi-scale outputs of the input feature map via a pyramid of pooling layers. The resulting feature maps, which form a hierarchy of features containing information at different scales and sub-regions, are then concatenated to produce an efficient prior global representation. Fig. 2c depicts the Pyramid Pooling Module in detail.

ColonFormer uses a decoder architecture inspired by UPerNet [37], which we denote as UPer Decoder. The decoder gradually fuses the prior global map produced by the PPM with multi-scale feature maps yielded by the MiT backbone. We suppose that applying convolutional layers to the feature maps of the MiT backbone is necessary since such layers can condense the information by emphasizing the coherence between neighboring elements and thus enhancing the resulting semantic map.

3.3 Refinement Module

The decoder’s outputs are further processed by a refinement module to achieve more precise and complete prediction maps. The refinement module consists of Channel-wise Feature Pyramid (CFP) module [38] (Fig. 2b) and our novel Reverse Attention module enhanced by a new residual axial attention block for incremental correction of polyp boundary [30, 39].

In the parallel reverse attention network architecture [23], the global map is derived from the deepest CNN layer, so it does not have many structural details and hence can present only rough locations of the polyp tissues. The proposed strategy to recover precise location and label is to exploit complementary regions and details in a sequential manner by removing previously estimated polyp regions from high-level side-output features, where the current estimation is up-sampled from the deeper layer. By using Reverse Attention, a coarse saliency map is guided to sequentially discover complement object regions and details by erasing the current predicted salient regions from side-output features. The current prediction is upsampled from its deeper layer. This erasing approach can refine the imprecise and coarse estimation into an accurate and complete prediction map. It was shown that self-attention layers in the MiT backbone work like low-pass filters. Therefore, we argue that using convolutional layers is important for the refinement module since such layers favor high-frequency components and can provide richer edge information for the boundary correction.

Inspired by CaraNet [40], we use Channel-wise Feature Pyramid (CFP) to extract features from the encoder in multi-scale views. As depicted in Fig. 2b, the CFP module has $K = 4$ branches with different dilation rates that allow them to capture information at multiple scales. However, a direct concatenation of all branches could lead to some unwanted checkerboard or gridding artifacts that significantly impact the quality of the following boundary correction. In order to avoid this issue, the CFP module combines these branches step by step to build a final accurate feature map to correct the polyp boundaries.

CaraNet [40] also enhanced the Reverse Attention module by an axial attention block, which is a straightforward generalization of self-attention that naturally aligns with the multiple dimensions of the tensors. This module is supposed to filter the necessary information for the refinement process. However, axial attention may not always be good for the network since it can accidentally eliminate important edge information. Therefore, we propose to relax this mechanism using an additional residual connection, which allows the network to omit the axial attention layers when required and thus facilitates the learning process. The novel refinement module is called Residual Axial Reverse Attention (RA-RA). We experimentally found that utilizing the RA-RA module up to the finest feature map does not help refine the polyp boundary better. Hence, we propose to use just three RA-RA blocks, as shown in Fig. 1. The effectiveness of the RA-RA module is investigated in detail in Section 4.4.

3.4 Loss Function

ColonFormer uses a compound loss combining the weighted focal loss and weighted IoU loss to train the model. The weighted focal loss is a distribution-based loss that treats every pixel individually. In contrast, the weighted IoU loss is a region-based loss that considers the relationships between neighboring pixels.

Image pixels can be easy to be correctly recognized. However, some pixels, such as those on the edge regions, may be harder to learn. Thus, the model should pay more attention to more challenging samples. In other words, some image pixels may be more important than others in contributing to the learning process. We represent the importance of pixel (i, j) by a weight β_{ij} . As suggested in [41], the weight β_{ij} for pixel (i, j) is defined as the difference between the center pixel and its neighbors:

$$\beta_{ij} = \left| \frac{\sum_{m,n \in \mathcal{N}_{ij}} g_{mn}}{|\mathcal{N}_{ij}|} - g_{ij} \right| \quad (1)$$

where \mathcal{N}_{ij} represents the area of 31×31 size surrounding the pixel (i, j) , and $g_{ij} \in \{0, 1\}$ is the true label of pixel (i, j) . A large value of β_{ij} indicates a pixel with considerable distinction from its vicinity, i.e., pixels at polyp edges. Such a weighting scheme enforces the model to focus more on the boundary regions.

Assume that p_{ij} is the prediction probability of the pixel (i, j) belonging the polyp class. Let us define q_{ij} as:

$$q_{ij} = \begin{cases} p_{ij}, & \text{if } g_{ij} = 1 \\ 1 - p_{ij}, & \text{otherwise} \end{cases} \quad (2)$$

As polyp segmentation is a problem with highly imbalanced data, focal loss is employed to deal with class imbalance during training. It integrates a modulating term in order to focus learning on hard pixels. The weighted focal loss is

Table 1: Performance comparison of different methods on the Kvasir, ClinicDB, ColonDB, CVC-T and ETIS-Larib test sets. All results of ColonFormer are averaged over five runs.

Method	Kvasir		CVC-ClinicDB		CVC-ColonDB		CVC-T		ETIS-Larib	
	mDice	mIOU	mDice	mIOU	mDice	mIOU	mDice	mIOU	mDice	mIOU
UNet [14]	0.818	0.746	0.823	0.750	0.512	0.444	0.710	0.627	0.398	0.335
UNet++ [15]	0.821	0.743	0.794	0.729	0.483	0.410	0.707	0.624	0.401	0.344
SFA [42]	0.723	0.611	0.700	0.607	0.469	0.347	0.297	0.217	0.467	0.329
PraNet [23]	0.898	0.840	0.899	0.849	0.709	0.640	0.871	0.797	0.628	0.567
HarDNet-MSEG [25]	0.912	0.857	0.932	0.882	0.731	0.660	0.887	0.821	0.677	0.613
CaraNet [40]	0.918	0.865	0.936	0.887	0.773	0.689	0.903	0.838	0.747	0.672
TransUNet [34]	0.913	0.857	0.935	0.887	0.781	0.699	0.893	0.824	0.731	0.660
TransFuse-L* [35]	0.920	0.870	0.942	0.897	<u>0.781</u>	0.706	<u>0.894</u>	<u>0.826</u>	0.737	0.663
ColonFormer-S (Ours)	0.927	0.877	<u>0.932</u>	0.883	0.811	<u>0.730</u>	<u>0.894</u>	<u>0.826</u>	<u>0.789</u>	<u>0.711</u>
ColonFormer-L (Ours)	<u>0.924</u>	<u>0.876</u>	<u>0.932</u>	<u>0.884</u>	0.811	0.733	0.906	0.842	0.801	0.722

then defined as follows:

$$\mathcal{L}_{wfocal} = - \frac{\sum_{i=1}^H \sum_{j=1}^W (1 + \lambda \beta_{ij}) \alpha (1 - q_{ij})^\gamma \log(q_{ij})}{\sum_{i=1}^H \sum_{j=1}^W (1 + \lambda \beta_{ij})} \quad (3)$$

where α, γ are tunable hyperparameters.

The weighted IoU loss is defined as follows:

$$\mathcal{L}_{wiou} = 1 - \frac{\sum_{i=1}^H \sum_{j=1}^W (g_{ij} * p_{ij}) * (1 + \lambda \beta_{ij})}{\sum_{i=1}^H \sum_{j=1}^W (g_{ij} + p_{ij} - g_{ij} * p_{ij}) * (1 + \lambda \beta_{ij})} \quad (4)$$

where λ is a hyperparameter to adjust the impact of importance weights β_{ij} .

The total loss of our ColonFormer is calculated as:

$$\mathcal{L}_{total} = \frac{\mathcal{L}_{wfocal} + \mathcal{L}_{wiou}}{2} \quad (5)$$

The total loss in Eq. (5) is applied to train our model for multi-scale outputs as shown in Fig. 1. The final loss is the sum of all total losses computed at different output levels. Note that each output is upsampled back to the original size of the image’s ground truth before the losses are evaluated.

4 Experiments

4.1 Datasets

We perform experiments on the five popular datasets for polyp segmentation: Kvasir [47], CVC-Clinic DB [48], CVC-Colon DB [49], CVC-T [50], and ETIS-Larib Polyp DB [51]. Details of these datasets are described as follows:

- **Kvasir dataset** is collected using endoscopic equipment at Vestre Viken Health Trust (VV), Norway. Images are carefully annotated and verified by experienced gastroenterologists from VV and the Cancer Registry of Norway. The dataset consists of 1000 images with different resolutions from 720×576 to 1920×1072 pixels.
- **CVC-ClinicDB dataset** is a database of frames extracted from colonoscopy videos. The dataset consists of 612 images with a resolution of 384×288 pixels from 31 colonoscopy sequences. The dataset was used in the training stages of the MICCAI 2015 Sub-Challenge on Automatic Polyp Detection Challenge in Colonoscopy Videos.
- **CVC-ColonDB dataset** is provided by the Machine Vision Group (MVG). The dataset consists of 380 images with a resolution of 574×500 pixels from 15 short colonoscopy videos.

Table 2: Performance comparison of different methods on 5-fold cross-validation of the CVC-ClinicDB and Kvasir datasets. All results are averaged over 5 folds.

Dataset	Method	mDice	mIOU	Recall	Precision
ClinicDB	UNet [14]	-	0.792	-	-
	MultiResUNet [43]	-	0.849	-	-
	ResUNet++ [44]	0.815 ± 0.018	0.736 ± 0.017	0.832 ± 0.018	0.830 ± 0.020
	DoubleUNet [16]	0.920 ± 0.018	0.866 ± 0.025	0.922 ± 0.027	0.928 ± 0.017
	DDANet [45]	0.860 ± 0.014	0.786 ± 0.017	0.858 ± 0.023	0.892 ± 0.014
	ColonSegNet [46]	0.817 ± 0.020	0.873 ± 0.024	0.926 ± 0.025	0.933 ± 0.014
	HarDNet-MSEG [25]	0.923 ± 0.020	0.873 ± 0.024	0.926 ± 0.025	0.933 ± 0.014
	PraNet [23]	0.933 ± 0.012	0.884 ± 0.015	0.940 ± 0.005	0.937 ± 0.016
	ColonFormer-S (Ours)	0.948 ± 0.002	0.904 ± 0.004	0.958 ± 0.003	0.941 ± 0.004
	ColonFormer-L (Ours)	0.947 ± 0.002	0.903 ± 0.003	0.956 ± 0.002	0.942 ± 0.005
Kvasir	UNet [14]	0.708 ± 0.017	0.602 ± 0.010	0.805 ± 0.014	0.716 ± 0.020
	ResUNet++ [44]	0.780 ± 0.010	0.681 ± 0.008	0.834 ± 0.010	0.799 ± 0.010
	DoubleUNet [16]	0.879 ± 0.018	0.816 ± 0.026	0.902 ± 0.027	0.894 ± 0.039
	DDANet [45]	0.860 ± 0.005	0.791 ± 0.004	0.876 ± 0.015	0.892 ± 0.018
	ColonSegNet [46]	0.676 ± 0.037	0.557 ± 0.040	0.731 ± 0.088	0.730 ± 0.080
	HarDNet-MSEG [25]	0.889 ± 0.011	0.831 ± 0.011	0.892 ± 0.015	0.926 ± 0.014
	PraNet [23]	0.883 ± 0.020	0.822 ± 0.020	0.897 ± 0.020	0.906 ± 0.010
	ColonFormer-S (Ours)	0.924 ± 0.008	0.875 ± 0.010	0.941 ± 0.010	0.927 ± 0.008
	ColonFormer-L (Ours)	0.917 ± 0.006	0.865 ± 0.007	0.932 ± 0.007	0.926 ± 0.008

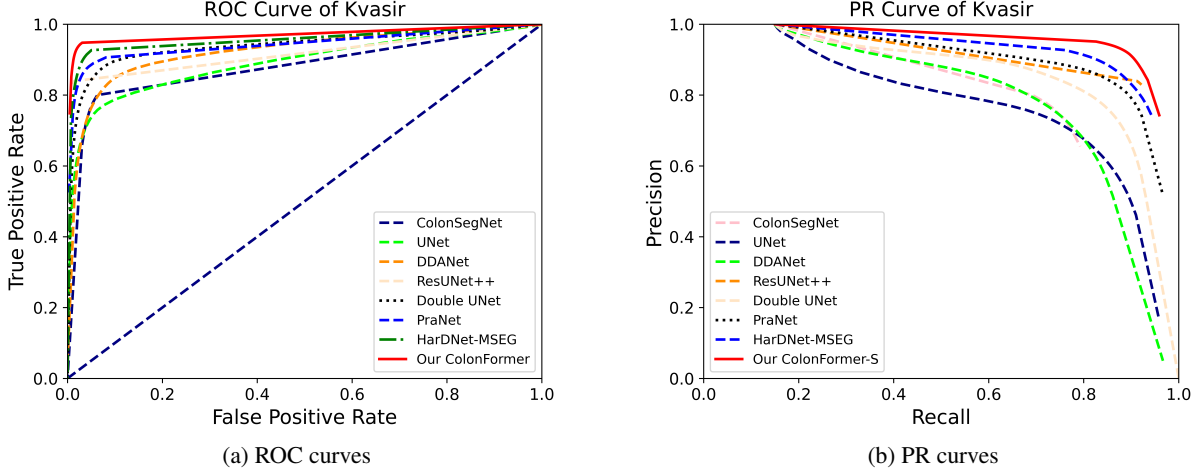


Figure 3: ROC curves and PR curves on the 5-fold cross-validation on the Kvasir-SEG dataset. All the curves are averaged over 5 folds.

- **CVC-T dataset** is the test set of a more extensive dataset called Endoscene. CVC-T consists of 60 images obtained from 44 video sequences acquired from 36 patients.
- **ETIS-Larib dataset** contains 196 high resolution (1226×996) colonoscopy images.

4.2 Experiment settings

We implement ColonFormer using the PyTorch framework. For a fair setting and comparison, we use the same parameters as [31] for the MiT backbone: kernel size $K = 7$, stride $S = 4$, padding size $P = 3$, and $K = 3, S = 2, P = 1$

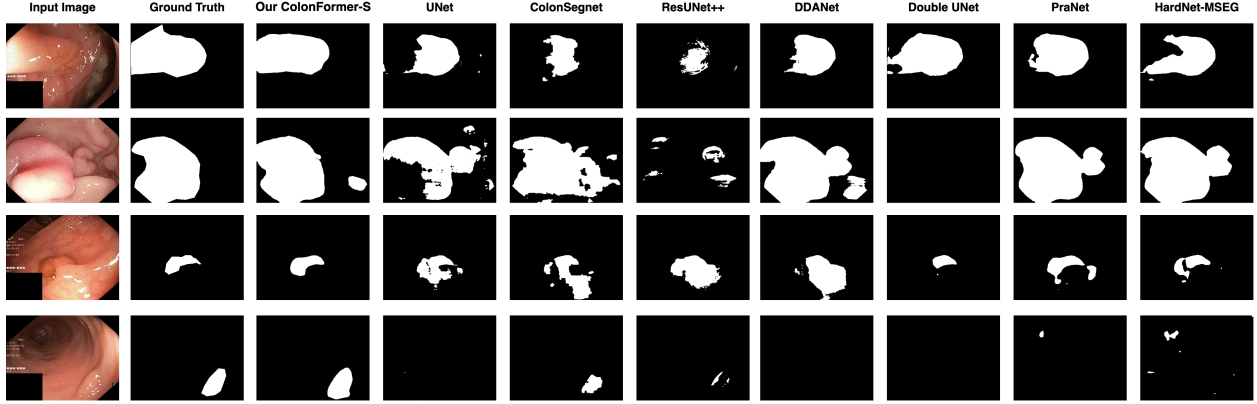


Figure 4: Qualitative result comparison of different models trained on the first fold of the 5-fold cross-validation on the Kvasir dataset.

Table 3: Performance comparison of different methods on cross-dataset configurations. All results are averaged over five runs.

Train	Test	Method	mDice	mIOU	Recall	Precision
CVC-ColonDB + ETIS-Larib	CVC-ClinicDB	ResUNet++ [44]	0.406	0.302	0.481	0.496
		ColonSegNet [46]	0.427	0.321	0.529	0.552
		DDANet [45]	0.624	0.515	0.697	0.692
		DoubleUNet [16]	0.738	0.651	0.758	0.824
		HarDNet-MSEG [25]	0.765	0.681	0.774	0.863
		PraNet [23]	0.779	0.689	0.832	0.812
		ColonFormer-S (Ours)	0.851	0.771	0.853	0.896
ColonFormer-L (Ours)	<u>0.847</u>	<u>0.770</u>	<u>0.844</u>	0.902		
CVC-ColonDB	CVC-ClinicDB	ResUNet++ [44]	0.339	0.247	0.380	0.484
		DoubleUNet [16]	0.441	0.375	0.423	0.639
		DDANet [45]	0.476	0.370	0.501	0.644
		ResNet101-Mask-RCNN [52]	0.641	0.565	0.646	0.725
		ColonSegNet [46]	0.582	0.268	0.511	0.460
		HarDNet-MSEG [25]	0.721	0.633	0.744	0.818
		PraNet [23]	0.738	0.647	0.751	0.832
		ColonFormer-S (Ours)	0.816	0.731	0.809	0.881
ColonFormer-L (Ours)	<u>0.804</u>	<u>0.723</u>	<u>0.794</u>	<u>0.877</u>		
CVC-ClinicDB	ETIS-Larib	ResUNet++ [44]	0.211	0.155	0.309	0.203
		ColonSegNet [46]	0.217	0.110	0.654	0.144
		DDANet [45]	0.400	0.313	0.507	0.464
		ResNet101-Mask-RCNN [52]	0.565	0.469	0.565	0.639
		DoubleUNet [16]	0.588	0.500	0.689	0.599
		PraNet [23]	0.631	0.555	0.762	0.597
		HarDNet-MSEG [25]	0.659	0.583	0.676	0.705
		ColonFormer-S (Ours)	<u>0.723</u>	<u>0.635</u>	<u>0.797</u>	<u>0.731</u>
		ColonFormer-L (Ours)	0.760	0.673	0.859	0.734

to produce features with the same size as the non-overlapping process. Based on experiments in [41], [53], we use $\lambda = 5$, $\alpha = 0.25$ and $\gamma = 2$ for the losses in Eq. (3) and Eq. (4). Training is performed using Google Colab on virtual machines with 16GB RAM and an NVIDIA Tesla P100 GPU. Input images are resized to 352×352 for testing. In

order to increase the model’s robustness w.r.t image sizes, the training images are consequently scaled with a factor of $\{0.75, 1, 1.25\}$, respectively, and fed to the model for learning. None of the data augmentation techniques is used in the training phase.

We use six experiment setups to evaluate our method; each setup is described in detail below:

- **Experiment 1:** We use the same split as suggested in [23], where 90% of the Kvasir and ClinicDB datasets are used for training. The remaining images in the Kvasir and CVC-ClinicDB datasets and all images from CVC-ColonDB, CVC-T, and ETIS-Larib are used for testing.
- **Experiment 2:** 5-fold cross-validation on the CVC-ClinicDB and Kvasir datasets. Each dataset is divided into five equal folds. Each run uses one fold for testing and four remaining folds for training.
- **Experiment 3:** Cross-dataset evaluation with 3 training-testing configurations:
 1. CVC-ColonDB and ETIS-Larib for training, CVC-ClinicDB for testing;
 2. CVC-ColonDB for training, CVC-ClinicDB for testing;
 3. CVC-ClinicDB for training, ETIS-Larib for testing.

The first experiment compares our ColonFormer model with state-of-the-art CNN-based and Transformer-based networks using the same widely-used dataset configuration as suggested in [23]. The second experiment compares ColonFormer’s learning ability to several recent polyp segmentation methods. Finally, the last experiment provides deeper insights into the generalization capability of ColonFormer and other benchmark models.

We use the Adam optimizer and cosine annealing scheduler with a learning rate of $1e-4$. ColonFormer is trained in 20 epochs with a batch size of 8. The checkpoint of the last epoch is used for evaluation. Except for the second experiment with 5-fold cross-validation, we train ColonFormer five times, and the ColonFormer’s results are averaged over five runs.

In addition, we perform a series of ablation studies to evaluate the effectiveness of each component in the proposed ColonFormer. All ablation studies are performed on the dataset configuration for Experiment 1.

4.3 Comparison with benchmark models

Table 1 describes the comparison results for Experiment 1. ColonFormer generally outperforms the benchmark models on most datasets. Notably, both ColonFormer-S and ColonFormer-L outperform the second-best TransFuse-L* by 3% in mDice and 2.7% in mIOU on the ColonDB dataset. Compared to the second-best CaraNet on the ETIS-Larib dataset, ColonFormer-S achieves an improvement of 5.2% in mDice, and 4.8% in mIOU, while ColonFormer-L achieves an improvement of 6.4% in mDice and 5.9% in mIOU. The high capacity of ColonFormer-L seems more suitable for the high resolution of images in the ETIS-Larib dataset. However, both ColonFormer-S and ColonFormer-L achieve roughly 1% lower metrics against TransFuse-L* on the CVC-ClinicDB dataset, whose images obtain very low resolution.

Table 2 describes the comparison results for Experiment 2. We report both the average value and the standard deviation for each metric, which reflects the models’ stability. One can see that both ColonFormer-S and ColonFormer-L outperform all other state-of-the-art models in mDice, mIOU, precision, and recall on both datasets. Notably, our ColonFormer is the most stable model on both datasets, achieving the lowest standard deviation for each evaluation metric.

Qualitative results for Experiment 2 are shown in Fig. 4. ColonFormer-S demonstrates much fewer wrongly predicted pixels in segmentation results than other models. ColonFormer-S also produces better ROC and PR curves than the benchmark models, as depicted in Fig. 3.

Table 3 describes the comparison results for Experiment 3. Overall, both ColonFormer-S and ColonFormer-L significantly outperform benchmark models on cross-dataset metrics. For the first configuration, ColonFormer-S outperforms the second-best PraNet by 7 – 8% on all metrics. In the second configuration, ColonFormer-S continues to achieve a 5.8% improvement in precision and 7.8% improvement in mDice over PraNet. For the third configuration, ColonFormer-L again shows its suitability to the ETIS-Larib dataset achieving a 10.1% improvement in mDice and 18.3% in recall over PraNet. These are highly significant improvements, showing that our ColonFormer can generalize very well to new unseen data. Some result samples for this experiment are shown in Fig. 5. Similar to Fig. 4, one can see that ColonFormer yields better segmentation results compared to other state-of-the-arts.

Table 4 compares ColonFormer with other benchmark models in terms of size and computational complexity. One can see that our ColonFormer-S obtains competitive size and computational complexity compared to the most lightweight

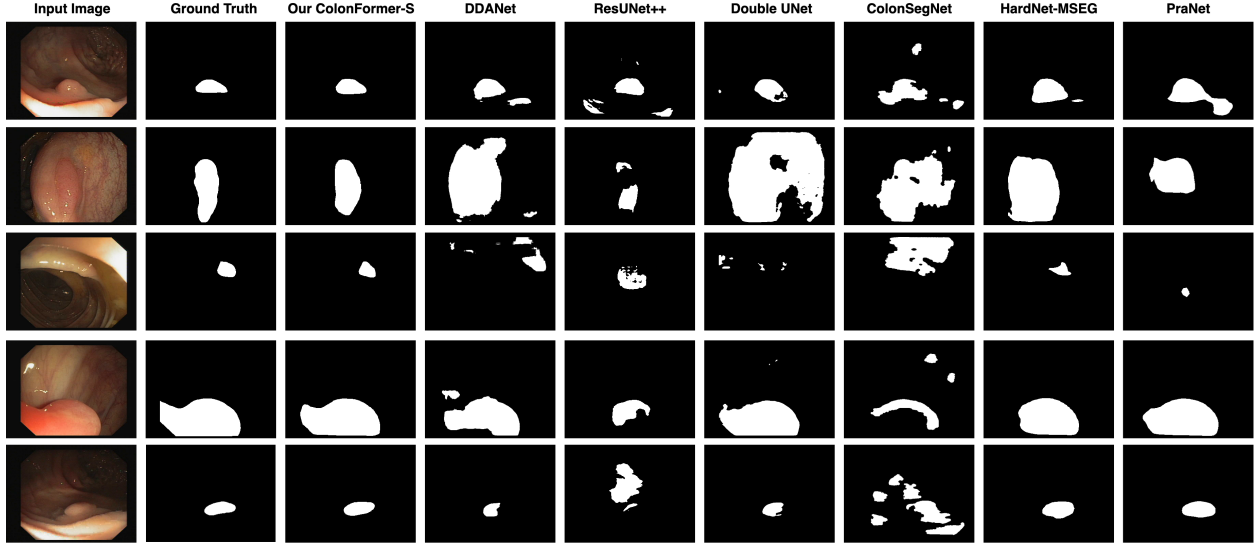


Figure 5: Qualitative result comparison using CVC-Colon for training and CVC-Clinic for testing.

CNN-based models such as PraNet [23], and HardNet-MSEG [25]. Our ColonFormer-L is larger than most CNN-based neural networks but still more efficient than other Transformer-based methods in terms of GFlops.

Table 4: Number of parameters and GFLOPs of different methods

Method	Parameters (M)	GFLOPs
PraNet [23]	32.55	13.11
HardNet-MSEG [25]	33.34	11.38
CaraNet [40]	46.64	21.69
TransUNet [34]	105.5	60.75
TransFuse-L* [35]	-	-
SegFormer-B3 [31]	47.22	33.68
SegFormer-B3-Uper	46.61	20.99
<i>ColonFormer-S (Ours)</i>	33.04	16.03
<i>ColonFormer-L (Ours)</i>	52.94	22.94

4.4 Ablation studies

Effectiveness of the UPer Decoder. We firstly compare the original SegFormer-B3 [31] with MLP Decoder and another model called SegFormer-B3-Uper that replaces the original MLP decoder with the UPer Decoder. Both models use the MiT-B3 backbone in terms of encoder. Results are shown in the first two rows of Table 5. Both network versions show similar metrics across the test datasets, with slight variations of roughly 1%. However, one can see from Table 4 that UPer Decoder is also significantly less costly, requiring only 20.99 GFLOPs as opposed to MLP Decoder (33.68 GFLOPs). These results compel us to choose the UPer decoder for ColonFormer, which alleviates the large computation costs incurred with the Transformer backbone.

Effectiveness of the Refinement Module. We evaluate the performance of SegFormer-B3-Uper-ARA with the A-RA Refinement Module as in [40], and our ColonFormer-L with the adjusted Refinement Module as described in Section 3.3. Results are shown in Table 5. Overall, incorporating the Refinement Module yields improvement across all datasets. Our ColonFormer-L also yields superior performance than SegFormer-B3-Uper-ARA on the Kvasir, CVC-ClinicDB, and most significantly, the ETIS-Larib datasets, while slightly underperforming on the CVC-ColonDB and CVC-T datasets.

Effectiveness of the MiT Backbone. The Mix Transformer (MiT) [31] backbone has several variations ranging from MiT-B0 to MiT-B5. Accordingly, our ColonFormer also have different variations, including ColonFormer-XS, ColonFormer-S, ColonFormer-L, ColonFormer-XL, ColonFormer-XXL, respectively. Table 6 shows our comparison

between all variations of ColonFormer. Overall, ColonFormer-S and ColonFormer-L yield the best average results across our test datasets.

Table 5: Ablation study on the effectiveness of different components. All results are averaged over five runs.

Method	Uper	A-RA	RA-RA	Kvasir		CVC-ClinicDB		CVC-ColonDB		CVC-T		ETIS-Larib	
				mDice	mIOU	mDice	mIOU	mDice	mIOU	mDice	mIOU	mDice	mIOU
SegFormer-B3 [31]	—	—	—	0.920	0.866	<u>0.925</u>	<u>0.876</u>	0.806	0.726	0.905	0.840	<u>0.786</u>	<u>0.707</u>
SegFormer-B3-Uper	✓	—	—	0.916	0.864	0.924	0.876	<u>0.811</u>	0.731	0.900	0.832	0.784	<u>0.707</u>
SegFormer-B3-Uper-ARA	✓	✓	—	<u>0.922</u>	<u>0.872</u>	0.922	0.875	0.812	0.734	<u>0.903</u>	<u>0.837</u>	0.787	0.704
ColonFormer-L (Ours)	✓	—	✓	0.924	0.876	0.932	0.884	<u>0.811</u>	<u>0.733</u>	0.906	0.842	0.801	0.722

Table 6: Evaluation metrics for different variations of the MiT backbone. All results are averaged over five runs.

Method	Backbone	Kvasir		CVC-ClinicDB		CVC-ColonDB		CVC-T		ETIS-Larib	
		mDice	mIOU	mDice	mIOU	mDice	mIOU	mDice	mIOU	mDice	mIOU
ColonFormer-XS	MiT-B1	0.913	0.859	0.926	0.876	0.784	0.700	0.879	0.808	0.758	0.679
ColonFormer-S	MiT-B2	0.927	0.877	0.932	<u>0.883</u>	<u>0.811</u>	0.730	0.894	0.826	0.789	0.711
ColonFormer-L	MiT-B3	<u>0.924</u>	<u>0.876</u>	0.932	0.884	<u>0.811</u>	<u>0.733</u>	0.906	0.842	0.801	0.722
ColonFormer-XL	MiT-B4	0.920	0.870	0.923	0.875	0.814	0.735	<u>0.905</u>	<u>0.840</u>	<u>0.795</u>	<u>0.715</u>
ColonFormer-XXL	MiT-B5	0.920	0.872	0.924	0.876	0.802	0.724	0.899	0.831	0.776	0.700

5 Conclusion

This paper proposes a novel deep neural network architecture called ColonFormer for colon polyp segmentation. Our model leverages both the advantages of Transformers and CNNs architectures to learn a powerful multi-scale hierarchical feature representation. We also enhance the reverse attention with axial attention by relaxing it with a residual connection. The refinement module allows the network to incrementally correct the polyp boundary from a coarse global map produced by the decoder. Our extensive experiments show that ColonFormer significantly outperforms existing state-of-the-art models on popular benchmark datasets.

In future works, we will investigate lightweight or sparse self-attention layers to reduce the computational complexity. In addition, other types of architectures for combining Transformers and CNNs can also be exploited.

6 Acknowledgments

This work was funded by Vingroup Innovation Foundation (VINIF) under project code VINIF.2020.DA17.

References

- [1] J. Bernal, N. Tajkbaksh, F. J. Sánchez, B. J. Matuszewski, H. Chen, L. Yu, Q. Angermann, O. Romain, B. Rustad, I. Balasingham, K. Pogorelov, S. Choi, Q. Debar, L. Maier-Hein, S. Speidel, D. Stoyanov, P. Brandao, H. Córdova, C. Sánchez-Montes, S. R. Gurudu, G. Fernández-Esparrach, X. Dray, J. Liang, and A. Histace. Comparative validation of polyp detection methods in video colonoscopy: Results from the miccai 2015 endoscopic vision challenge. *IEEE Transactions on Medical Imaging*, 36(6):1231–1249, 2017.
- [2] Douglas A Corley, Christopher D Jensen, Amy R Marks, Wei K Zhao, Jeffrey K Lee, Chyke A Doubeni, Ann G Zauber, Jolanda de Boer, Bruce H Fireman, Joanne E Schottinger, et al. Adenoma detection rate and risk of colorectal cancer and death. *New england journal of medicine*, 370(14):1298–1306, 2014.
- [3] AM Leufkens, MGH Van Oijen, FP Vleggaar, and PD Siersema. Factors influencing the miss rate of polyps in a back-to-back colonoscopy study. *Endoscopy*, 44(05):470–475, 2012.
- [4] Pablo Mesejo, Daniel Pizarro, Armand Abergel, Olivier Rouquette, Sylvain Beorchia, Laurent Poincloux, and Adrien Bartoli. Computer-aided classification of gastrointestinal lesions in regular colonoscopy. *IEEE transactions on medical imaging*, 35(9):2051–2063, 2016.
- [5] Guanyu Zhou, Xiaogang Liu, Tyler M Berzin, Jeremy R Glissen Brown, Liangping Li, Chao Zhou, Zhenzhen Guo, Lei Lei, Fei Xiong, Yan Pan, et al. 951e—a real-time automatic deep learning polyp detection system

- increases polyp and adenoma detection during colonoscopy: a prospective double-blind randomized study. *Gastroenterology*, 156(6):S-1511, 2019.
- [6] Shin-ei Kudo, Yuichi Mori, Masashi Misawa, Kenichi Takeda, Toyoki Kudo, Hayato Itoh, Masahiro Oda, and Kensaku Mori. Artificial intelligence and colonoscopy: Current status and future perspectives. *Digestive Endoscopy*, 31(4):363–371, 2019.
- [7] Peng-Jen Chen, Meng-Chiung Lin, Mei-Ju Lai, Jung-Chun Lin, Henry Horng-Shing Lu, and Vincent S Tseng. Accurate classification of diminutive colorectal polyps using computer-aided analysis. *Gastroenterology*, 154(3):568–575, 2018.
- [8] Raf Bisschops, James E East, Cesare Hassan, Yark Hazewinkel, Michał F Kamiński, Helmut Neumann, Maria Pellisé, Giulio Antonelli, Marco Bustamante Balen, Emmanuel Coron, et al. Advanced imaging for detection and differentiation of colorectal neoplasia: European society of gastrointestinal endoscopy (esge) guideline–update 2019. *Endoscopy*, 51(12):1155–1179, 2019.
- [9] Ashish Vaswani, Noam Shazeer, Niki Parmar, Jakob Uszkoreit, Llion Jones, Aidan N Gomez, Łukasz Kaiser, and Illia Polosukhin. Attention is all you need. *Advances in neural information processing systems*, 30, 2017.
- [10] Ze Liu, Yutong Lin, Yue Cao, Han Hu, Yixuan Wei, Zheng Zhang, Stephen Lin, and Baining Guo. Swin transformer: Hierarchical vision transformer using shifted windows. In *Proceedings of the IEEE/CVF International Conference on Computer Vision*, pages 10012–10022, 2021.
- [11] Wenhai Wang, Enze Xie, Xiang Li, Deng-Ping Fan, Kaitao Song, Ding Liang, Tong Lu, Ping Luo, and Ling Shao. Pyramid vision transformer: A versatile backbone for dense prediction without convolutions. In *Proceedings of the IEEE/CVF International Conference on Computer Vision*, pages 568–578, 2021.
- [12] René Ranftl, Alexey Bochkovskiy, and Vladlen Koltun. Vision transformers for dense prediction. In *Proceedings of the IEEE/CVF International Conference on Computer Vision*, pages 12179–12188, 2021.
- [13] Sixiao Zheng, Jiachen Lu, Hengshuang Zhao, Xi Tian Zhu, Zekun Luo, Yabiao Wang, Yanwei Fu, Jianfeng Feng, Tao Xiang, Philip HS Torr, et al. Rethinking semantic segmentation from a sequence-to-sequence perspective with transformers. In *Proceedings of the IEEE/CVF conference on computer vision and pattern recognition*, pages 6881–6890, 2021.
- [14] Olaf Ronneberger, Philipp Fischer, and Thomas Brox. U-net: Convolutional networks for biomedical image segmentation. In *International Conference on Medical image computing and computer-assisted intervention*, pages 234–241. Springer, 2015.
- [15] Zongwei Zhou, Md Mahfuzur Rahman Siddiquee, Nima Tajbakhsh, and Jianming Liang. Unet++: A nested u-net architecture for medical image segmentation. In *Deep learning in medical image analysis and multimodal learning for clinical decision support*, pages 3–11. Springer, 2018.
- [16] Debesh Jha, Michael A Riegler, Dag Johansen, Pål Halvorsen, and Håvard D Johansen. Doubleu-net: A deep convolutional neural network for medical image segmentation. In *2020 IEEE 33rd International symposium on computer-based medical systems (CBMS)*, pages 558–564. IEEE, 2020.
- [17] Liang-Chieh Chen, George Papandreou, Iasonas Kokkinos, Kevin Murphy, and Alan L Yuille. Deeplab: Semantic image segmentation with deep convolutional nets, atrous convolution, and fully connected crfs. *IEEE transactions on pattern analysis and machine intelligence*, 40(4):834–848, 2017.
- [18] Jie Hu, Li Shen, and Gang Sun. Squeeze-and-excitation networks. In *Proceedings of the IEEE conference on computer vision and pattern recognition*, pages 7132–7141, 2018.
- [19] Karen Simonyan and Andrew Zisserman. Very deep convolutional networks for large-scale image recognition. *arXiv preprint arXiv:1409.1556*, 2014.
- [20] Andrew G Howard, Menglong Zhu, Bo Chen, Dmitry Kalenichenko, Weijun Wang, Tobias Weyand, Marco Andreetto, and Hartwig Adam. Mobilenets: Efficient convolutional neural networks for mobile vision applications. *arXiv preprint arXiv:1704.04861*, 2017.
- [21] Kaiming He, Xiangyu Zhang, Shaoqing Ren, and Jian Sun. Deep residual learning for image recognition. In *Proceedings of the IEEE conference on computer vision and pattern recognition*, pages 770–778, 2016.
- [22] Gao Huang, Zhuang Liu, Laurens Van Der Maaten, and Kilian Q Weinberger. Densely connected convolutional networks. In *Proceedings of the IEEE conference on computer vision and pattern recognition*, pages 4700–4708, 2017.
- [23] Deng-Ping Fan, Ge-Peng Ji, Tao Zhou, Geng Chen, Huazhu Fu, Jianbing Shen, and Ling Shao. Pranet: Parallel reverse attention network for polyp segmentation. In *International Conference on Medical Image Computing and Computer-Assisted Intervention*, pages 263–273. Springer, 2020.

- [24] Dinh Viet Sang, Tran Quang Chung, Phan Ngoc Lan, Dao Viet Hang, Dao Van Long, and Nguyen Thi Thuy. Ag-curesnest: A novel method for colon polyp segmentation. *arXiv preprint arXiv:2105.00402*, 2021.
- [25] Chien-Hsiang Huang, Hung-Yu Wu, and Youn-Long Lin. Hardnet-mseg: A simple encoder-decoder polyp segmentation neural network that achieves over 0.9 mean dice and 86 fps. *arXiv preprint arXiv:2101.07172*, 2021.
- [26] Phan Ngoc Lan, Nguyen Sy An, Dao Viet Hang, Dao Van Long, Tran Quang Trung, Nguyen Thi Thuy, and Dinh Viet Sang. Neounet: Towards accurate colon polyp segmentation and neoplasm detection. In *International Symposium on Visual Computing*, pages 15–28. Springer, 2021.
- [27] Nguyen S An, Phan N Lan, Dao V Hang, Dao V Long, Tran Q Trung, Nguyen T Thuy, and Dinh V Sang. Blazeneo: Blazing fast polyp segmentation and neoplasm detection. *IEEE Access*, 2022.
- [28] Jo Schlemper, Ozan Oktay, Michiel Schaap, Mattias Heinrich, Bernhard Kainz, Ben Glocker, and Daniel Rueckert. Attention gated networks: Learning to leverage salient regions in medical images. *Medical image analysis*, 53:197–207, 2019.
- [29] Nguyen Ba Hung, Nguyen Thanh Duc, Thai Van Chien, and Dinh Viet Sang. Ag-resunet++: An improved encoder-decoder based method for polyp segmentation in colonoscopy images. In *2021 RIVF International Conference on Computing and Communication Technologies (RIVF)*, pages 1–6. IEEE, 2021.
- [30] Shuhan Chen, Xiuli Tan, Ben Wang, and Xuelong Hu. Reverse attention for salient object detection. In *Proceedings of the European conference on computer vision (ECCV)*, pages 234–250, 2018.
- [31] Enze Xie, Wenhai Wang, Zhiding Yu, Anima Anandkumar, Jose M Alvarez, and Ping Luo. Segformer: Simple and efficient design for semantic segmentation with transformers. *Advances in Neural Information Processing Systems*, 34, 2021.
- [32] Alexander Kolesnikov, Alexey Dosovitskiy, Dirk Weissenborn, Georg Heigold, Jakob Uszkoreit, Lucas Beyer, Matthias Minderer, Mostafa Dehghani, Neil Houlsby, Sylvain Gelly, Thomas Unterthiner, and Xiaohua Zhai. An image is worth 16x16 words: Transformers for image recognition at scale. In *9th International Conference on Learning Representations, ICLR 2021, Virtual Event, Austria, May 3-7, 2021*, 2021.
- [33] Hugo Touvron, Matthieu Cord, Matthijs Douze, Francisco Massa, Alexandre Sablayrolles, and Hervé Jégou. Training data-efficient image transformers & distillation through attention. In *International Conference on Machine Learning*, pages 10347–10357. PMLR, 2021.
- [34] Jieneng Chen, Yongyi Lu, Qihang Yu, Xiangde Luo, Ehsan Adeli, Yan Wang, Le Lu, Alan L Yuille, and Yuyin Zhou. Transunet: Transformers make strong encoders for medical image segmentation. *arXiv preprint arXiv:2102.04306*, 2021.
- [35] Yundong Zhang, Huiye Liu, and Qiang Hu. Transfuse: Fusing transformers and cnns for medical image segmentation. In *International Conference on Medical Image Computing and Computer-Assisted Intervention*, pages 14–24. Springer, 2021.
- [36] Hengshuang Zhao, Jianping Shi, Xiaojuan Qi, Xiaogang Wang, and Jiaya Jia. Pyramid scene parsing network. In *Proceedings of the IEEE conference on computer vision and pattern recognition*, pages 2881–2890, 2017.
- [37] Tete Xiao, Yingcheng Liu, Bolei Zhou, Yuning Jiang, and Jian Sun. Unified perceptual parsing for scene understanding. In *Proceedings of the European Conference on Computer Vision (ECCV)*, pages 418–434, 2018.
- [38] Ange Lou and Murray Loew. Cfpnet: channel-wise feature pyramid for real-time semantic segmentation. In *2021 IEEE International Conference on Image Processing (ICIP)*, pages 1894–1898. IEEE, 2021.
- [39] Jonathan Ho, Nal Kalchbrenner, Dirk Weissenborn, and Tim Salimans. Axial attention in multidimensional transformers. *arXiv preprint arXiv:1912.12180*, 2019.
- [40] Ange Lou, Shuyue Guan, and Murray Loew. Caranet: Context axial reverse attention network for segmentation of small medical objects. *arXiv preprint arXiv:2108.07368*, 2021.
- [41] Jun Wei, Shuhui Wang, and Qingming Huang. F³net: Fusion, feedback and focus for salient object detection. In *Proceedings of the AAAI Conference on Artificial Intelligence*, volume 34, pages 12321–12328, 2020.
- [42] Yuqi Fang, Cheng Chen, Yixuan Yuan, and Kai-yu Tong. Selective feature aggregation network with area-boundary constraints for polyp segmentation. In *International Conference on Medical Image Computing and Computer-Assisted Intervention*, pages 302–310. Springer, 2019.
- [43] Nabil Ibtehaz and M Sohel Rahman. Multiresunet: Rethinking the u-net architecture for multimodal biomedical image segmentation. *Neural Networks*, 121:74–87, 2020.
- [44] Debesh Jha, Pia H Smedsrud, Michael A Riegler, Dag Johansen, Thomas De Lange, Pål Halvorsen, and Håvard D Johansen. Resunet++: An advanced architecture for medical image segmentation. In *2019 IEEE International Symposium on Multimedia (ISM)*, pages 225–2255. IEEE, 2019.

- [45] Nikhil Kumar Tomar, Debesh Jha, Sharib Ali, Håvard D Johansen, Dag Johansen, Michael A Riegler, and Pål Halvorsen. Ddanet: Dual decoder attention network for automatic polyp segmentation. In *ICPR International Workshop and Challenges*, 2021.
- [46] Debesh Jha, Sharib Ali, Nikhil Kumar Tomar, Håvard D Johansen, Dag Johansen, Jens Rittscher, Michael A Riegler, and Pål Halvorsen. Real-time polyp detection, localization and segmentation in colonoscopy using deep learning. *Ieee Access*, 9:40496–40510, 2021.
- [47] Debesh Jha, Pia H Smedsrud, Michael A Riegler, Pål Halvorsen, Thomas de Lange, Dag Johansen, and Håvard D Johansen. Kvasir-seg: A segmented polyp dataset. In *International Conference on Multimedia Modeling*, pages 451–462. Springer, 2020.
- [48] Jorge Bernal, F Javier Sánchez, Gloria Fernández-Esparrach, Debora Gil, Cristina Rodríguez, and Fernando Vilarinho. Wm-dova maps for accurate polyp highlighting in colonoscopy: Validation vs. saliency maps from physicians. *Computerized Medical Imaging and Graphics*, 43:99–111, 2015.
- [49] Nima Tajbakhsh, Suryakanth R Gurudu, and Jianming Liang. Automated polyp detection in colonoscopy videos using shape and context information. *IEEE transactions on medical imaging*, 35(2):630–644, 2015.
- [50] David Vázquez, Jorge Bernal, F Javier Sánchez, Gloria Fernández-Esparrach, Antonio M López, Adriana Romero, Michal Drozdal, and Aaron Courville. A benchmark for endoluminal scene segmentation of colonoscopy images. *Journal of healthcare engineering*, 2017, 2017.
- [51] Juan Silva, Aymeric Histace, Olivier Romain, Xavier Dray, and Bertrand Granado. Toward embedded detection of polyps in wce images for early diagnosis of colorectal cancer. *International journal of computer assisted radiology and surgery*, 9(2):283–293, 2014.
- [52] Hemin Ali Qadir, Younghak Shin, Johannes Solhusvik, Jacob Bergsland, Lars Aabakken, and Ilanko Balasingham. Polyp detection and segmentation using mask r-cnn: Does a deeper feature extractor cnn always perform better? In *2019 13th International Symposium on Medical Information and Communication Technology (IS-MICT)*, pages 1–6. IEEE, 2019.
- [53] Tsung-Yi Lin, Priya Goyal, Ross Girshick, Kaiming He, and Piotr Dollár. Focal loss for dense object detection. In *Proceedings of the IEEE international conference on computer vision*, pages 2980–2988, 2017.